

Searching for photon-sector Lorentz violation using gravitational-wave detectors

V. Alan Kostelecký,¹ Adrian C. Melissinos,² and Matthew Mewes³

¹*Physics Department, Indiana University, Bloomington, Indiana 47405, USA*

²*Department of Physics and Astronomy, University of Rochester, Rochester, New York 14627, USA*

³*Physics Department, California Polytechnic State University, San Luis Obispo, California 93407, USA*

IUHET 612, July 2016; published in Physics Letters B, DOI:10.1016/j.physletb.2016.08.001

Abstract

We study the prospects for using interferometers in gravitational-wave detectors as tools to search for photon-sector violations of Lorentz symmetry. Existing interferometers are shown to be exquisitely sensitive to tiny changes in the effective refractive index of light occurring at frequencies around and below the microhertz range, including at the harmonics of the frequencies of the Earth's sidereal rotation and annual revolution relevant for tests of Lorentz symmetry. We use preliminary data obtained by the Laser Interferometer Gravitational-Wave Observatory (LIGO) in 2006-2007 to place constraints on coefficients for Lorentz violation in the photon sector exceeding current limits by about four orders of magnitude.

Interferometry has been a valuable tool for investigating relativity for well over a century, beginning with the classic Michelson-Morley and Kennedy-Thorndike experiments [1, 2] that helped to establish the underlying Lorentz symmetry of relativity. The suggestion that tiny deviations from Lorentz invariance could arise from an underlying unified theory such as strings [3] has revitalized experimental efforts to probe relativity in recent years, leading to many sensitive searches for Lorentz violation involving interferometric experiments with light, particles, and atoms [4]. Recently, the relativistic prediction of gravitational waves has been confirmed using interferometric techniques [5].

The world's largest laser interferometers are associated with gravitational-wave observatories, and it is natural to ask about their potential sensitivity to Lorentz-violating effects involving photons. Existing observatories include the Laser Interferometer Gravitational-Wave Observatory (LIGO) [6] with interferometers located at Hanford, Washington and Livingston, Louisiana, and the Virgo observatory [7] with interferometer located near Pisa, Italy. Other large ground-based observatories are operational or planned [8–10], and efforts to develop a space-based observatory, the Laser Interferometer Space Antenna (LISA) [11] are underway. Here, we examine the potential for using low-frequency data from these interferometers to search for signals of Lorentz violation in the form of rotation and boost asymmetries associated with the sidereal rotation and annual revolution of the Earth. We present a general theoretical framework for discussing the effects, and we apply it to preliminary LIGO data collected in 2006-2007 with the Hanford instrument. The results obtained below reveal an attained sensitivity to Lorentz violation in the photon sector about four orders of magnitude greater than current laboratory experiments.

A rough estimate of the sensitivity of the gravitational-wave instruments can be made by noting that each can be idealized

as a Michelson interferometer with Fabry-Pérot cavities in the arms. At LIGO, for example, the physical size of each arm is $L \simeq 4$ km, with an effective path length for the laser light of about 1000 km due to the cavity finesse $F \simeq 280$ for the configuration during the 2006-2007 run. The laser operates at an infrared wavelength $\lambda \simeq 1064$ nm, and the relative fringe shift S can be measured to $S \simeq 4 \times 10^{-10}$. Taken together, these values suggest that an effective sensitivity to a shift δf of the frequency f of $\delta f/f \approx S \lambda / FL \simeq 4 \times 10^{-22}$ is attainable. This estimate suggests that gravitational-wave observatories potentially have intrinsic sensitivities to Lorentz violation several orders of magnitude better than those achieved in recent Michelson-Morley experiments [4, 12–14]. It thus provides motivation for the present investigation of the prospects for tests of Lorentz symmetry with LIGO and other gravitational-wave interferometers.

The LIGO interferometer is optimized for detection of gravitational-wave signals in the approximate range 40-1000 Hz. The measured signal at the detector port can be taken as the net phase shift

$$\Delta\phi = \delta\phi_1 - \delta\phi_2 \quad (1)$$

arising from the individual phase shifts $\delta\phi_j$, $j = 1, 2$, experienced by the light in each of the two arms. These individual phase shifts can in principle arise from changes δL_j in the effective path lengths L_j of the arms, or a change δf_c in the carrier frequency f_c of the light. The phase shifts can also be affected by modifications $\delta\bar{n}_j$ of the effective refractive index \bar{n} experienced by the light propagating in the two arms, including changes that might arise due to the presence of Lorentz violation. The net phase shift on the j th arm for a single light traversal of length $2L$ can thus be expressed as

$$\frac{\delta\phi_j}{2\pi} = \left(\frac{\delta L_j}{L} + \frac{\delta f_c}{f_c} + \frac{\delta\bar{n}_j}{\bar{n}} \right) \frac{2L}{\lambda}. \quad (2)$$

In its operating mode, the interferometer is ‘locked’ on a dark fringe by adjusting the carrier frequency f_c and the effective path lengths L_j using feedback and servo mechanisms, so that $\Delta\phi = 0$ is enforced at the detector port in the absence of a gravitational-wave signal. Over a sufficiently large time interval T compared to the time between successive feedback and servo actions, the integrated net phase change reduces to an integral over changes in the difference $\Delta\bar{n} = \delta\bar{n}_1 - \delta\bar{n}_2$ of effective refractive indices,

$$\int_{t-T/2}^{t+T/2} dt \frac{\Delta\phi_j}{2\pi} \rightarrow \frac{2L}{\lambda} \int_{t-T/2}^{t+T/2} dt \frac{\Delta\bar{n}}{\bar{n}}, \quad (3)$$

because the changes δL_j and δf_c are stochastic and average to zero when the interferometer is locked.

The above reasoning demonstrates that the operating mode of the interferometer does in principle have sensitivity to time-varying signals from Lorentz violation in the effective refractive index \bar{n} . However, the Earth’s sidereal-rotation angular frequency is $\omega_\oplus \simeq 7.3 \times 10^{-5}$ rad Hz, while its annual-revolution angular frequency is $\Omega_\oplus \simeq 2.0 \times 10^{-7}$ rad Hz, so the sidereal and annual signals of interest for searches for Lorentz violation involve frequencies many orders of magnitude below the optimized band of the instrument. At these low frequencies, the instrumental noise makes clean extraction of any signal challenging. One possible option for sidestepping this issue is to take advantage of information circulating in the interferometer at sideband frequencies, as we discuss next.

The arms are in resonance when the carrier frequency f_c takes the value $f_c = N f_{\text{fsr}}$, where N is typically a large integer of order 10^{10} and $f_{\text{fsr}} = c/2L \simeq 37.52$ kHz at LIGO is called the free spectral range (fsr) frequency. Resonance also occurs at the sidebands $f_\pm = f_c \pm f_{\text{fsr}}$, which experience lower noise and are thus interesting candidates for signal analysis. Furthermore, a *macroscopic* difference $\Delta L = L_1 - L_2$ in the arm lengths, which for LIGO is of order 2 cm, displaces these sidebands from the dark fringe by a bias phase shift $\phi_b = \pm \Delta L/2L \simeq 3 \times 10^{-6}$ per traversal of the light. This implies that the power at the detector port at the sideband frequency f_+ contains an interference term between the bias phase shift and any phase shift from the change (3) in the difference $\Delta\bar{n}$ of effective refractive indices. The power at f_+ is thus modulated at the frequencies of harmonic changes in $\Delta\bar{n}$. In short, when the carrier frequency is used to lock the interferometer, the sideband at the fsr frequency can be used to measure the low-frequency signals from Lorentz violation [15, 16].

A successful measurement of harmonic changes in $\Delta\bar{n}$ associated with tidal forces has already been demonstrated [17]. The tidal acceleration has a gravity-gradient component g_h along the interferometer arms that induces redshifts in the circulating light. The redshifts act to produce effective changes in $\Delta\bar{n}$ varying harmonically at the tidal frequencies and introduce a single-traversal phase shift of

$$\frac{\delta\phi}{2\pi} = \frac{g_h L^2}{\lambda c^2}. \quad (4)$$

Using preliminary LIGO data from the 2006-2007 run [15], the spectral powers at the tidal frequencies are found to be in ap-

proximate agreement with results from standard modeling of the tidal gradients. Note that the tidal frequencies also appear in the demodulated carrier signal at the detector port but are compromised by noise, while they are observable at their exact frequencies in the spectrum obtained from the fsr signal.

To investigate possible signals from Lorentz violation, we adopt here the methods of effective field theory, which provide powerful and model-independent techniques for studying observable signals originating from an otherwise unattainable large energy scale [18]. The realistic effective field theory describing general Lorentz violation is called the Standard-Model Extension (SME) [19, 20]. It is constructed by adding Lorentz-violating terms to the action for General Relativity coupled to the Standard Model. Each addition to the Lagrange density is a coordinate-independent contraction of a Lorentz-violating operator with a coefficient determining the size of its physical effects. Any operator can be classified according to its mass dimension d in natural units, with the corresponding coefficient having mass dimension $4 - d$. Operators of larger d can plausibly be interpreted as representing effects at higher order in a low-energy expansion of the underlying theory. In Minkowski spacetime, limiting attention to terms with $d \leq 4$ produces a theory that is power-counting renormalizable and known as the minimal SME. Reviews include, for example, Refs. [4, 21, 22].

In the present work, we focus attention on possible effects from the photon sector of the SME. We analyze potential signals at harmonics of the sidereal frequency ω_\oplus and the annual frequency Ω_\oplus , including the sidebands. In principle, Lorentz-violating contributions to the signal could also arise from the matter sector, including in particular from the electrons, protons, and neutrons in the interferometer mirrors. While of definite interest, addressing this possibility would complicate the present analysis without contributing to our goal of demonstrating that gravitational-wave detectors have competitive sensitivity to Lorentz violation, and so we defer it to future investigation. This obviates the issue of fixing possible field redefinitions and coordinate choices [19, 20, 23–25]. We also simplify the analysis by disregarding contributions to Lorentz-violating birefringence of light, as disentangling these effects requires unavailable information about the polarization of the light circulating in the interferometer.

The possible modifications to the effective refractive index for photons propagating in the presence of Lorentz violation have been classified and enumerated for arbitrary d [24]. Non-birefringent Lorentz-violating operators in the photon sector appear only for even $d \geq 4$. Decomposing in spherical harmonics implies the corresponding spherical coefficients for Lorentz violation can be denoted by $c_{(I)jm}^{(d)}$, where the subscript I indicates nonbirefringence and the indices jm are the usual angular quantum numbers for the spherical harmonics with $j \leq d - 2$. All the associated modifications to the effective refractive index can then be expressed in the form [24]

$$n = 1 + \zeta^0, \quad \zeta^0 = \sum_{d,jm} E^{d-4} (-1)^j Y_{jm}(\hat{l}) c_{(I)jm}^{(d)\text{lab}}, \quad (5)$$

where E is the photon energy, \hat{l} is the direction of its momentum, $c_{(I)jm}^{(d)\text{lab}}$ are the coefficients for Lorentz violation seen in the

laboratory frame, and $d \geq 4$ takes only even values.

To apply the above results in the context of LIGO, consider first a single arm of the interferometer. For a traversal of the light down the arm and back, we can introduce an averaged refractive index

$$\begin{aligned}\bar{n}(\hat{l}) &= \frac{1}{2}(\zeta^0(\hat{l}) + \zeta^0(-\hat{l})) \\ &= 1 + \sum_{d,jm} E^{d-4} \frac{1}{2}(1 + (-1)^j) Y_{jm}(\hat{l}) c_{(I)jm}^{(d)\text{lab}}.\end{aligned}\quad (6)$$

Taking both arms into account, the difference $\Delta\bar{n}$ appearing in Eq. (3) is then given by

$$\Delta\bar{n} = \bar{n}(\hat{l}_1) - \bar{n}(\hat{l}_2), \quad (7)$$

where the angle between \hat{l}_1 and \hat{l}_2 can be taken as $\pi/2$.

The LIGO observatory is a noninertial frame due to the rotation and revolution of the Earth. In searching for Lorentz violation, it is useful to work instead in a frame that is approximately inertial over the time period of the experiment. The canonical choice for this inertial frame is the Sun-centered frame [4, 25, 26], with coordinates denoted as (T, X, Y, Z) . The origin of the time T is defined to be the vernal equinox 2000, so that $T(2000-03-20\ 07:35\ \text{UTC}) = 0$. The Z axis is aligned with the Earth's rotation axis, and the X axis points towards the vernal equinox 2000. The coefficients $c_{(I)jm}^{(d)}$ can plausibly be assumed constant on solar-system scales in this frame [19]. The rotation and revolution of the Earth thus induce sidereal and annual variations in the laboratory coefficients $c_{(I)jm}^{(d)\text{lab}}$. These variations are key signals for detecting Lorentz violation.

Consider first sidereal variations. The spherical coefficients $c_{(I)jm}^{(d)}$ for Lorentz violation are particularly well suited for studies of sidereal signals because they transform under rotations in a comparatively simple way. The relationship between the spherical coefficients in the laboratory frame and ones in the Sun-centered frame is given by [24]

$$c_{(I)jm}^{(d)\text{lab}} = \sum_{m'} e^{im'\omega_\oplus T_\oplus} d_{mm'}^j(-\chi) c_{(I)jm'}^{(d)}, \quad (8)$$

where χ is the colatitude of the laboratory and the little Wigner matrices $d_{mm'}^j$ are specified in Eq. (136) of Ref. [24]. The time $T_\oplus = T - T_0$ is a local sidereal time, offset from T by $T_0 \simeq (23.934\ \text{hr})(66.25^\circ - \lambda)/360^\circ$, where λ is the longitude of the laboratory in degrees. For the Hanford site, $\chi \simeq 43.5^\circ$ and $T_0 \simeq 2000-03-20\ 19:56\ \text{UTC}$.

Substituting the result (8) into the difference (7) gives

$$\Delta\bar{n} = \sum_{d,jmm'} \mathcal{M}_{(I)jm}^{(d)\text{lab}} e^{im'\omega_\oplus T_\oplus} d_{mm'}^j(-\chi) c_{(I)jm'}^{(d)}. \quad (9)$$

In this expression, the experiment-dependent factor $\mathcal{M}_{(I)jm}^{(d)\text{lab}}$ is given by

$$\mathcal{M}_{(I)jm}^{(d)\text{lab}} = E^{d-4} \frac{1}{2}(1 + (-1)^j)(1 - i^m) Y_{jm}(\frac{\pi}{2}, \phi), \quad (10)$$

where ϕ is the angle of the interferometer 'X' arm measured east of south, which is $\phi \simeq -144^\circ$ for the interferometer at the Hanford site. As an example, Table 1 displays the explicit numerical form of the combinations (9) for harmonics with $d = 4$

and $d = 6$ for this site. The first column shows the harmonic. The second column contains the combination for $d = 4$ contributing to the difference $\Delta\bar{n}$. The third column lists the combinations contributing for $d = 6$. The numerical factors in this last column are given in units of $10^{-18}\ \text{GeV}^2$. The contributions to $\Delta\bar{n}$ from an individual harmonic can be obtained from this table by multiplying an entry in the first column with one in the second or third column.

Next, consider annual variations. These are associated with boosts between the Sun-centered and laboratory frames, so working with cartesian coefficients for Lorentz violation is conceptually more straightforward than spherical coefficients. To keep the analysis comparatively simple we focus here on the case $d = 4$, for which the effects are unsuppressed by powers of the energy E . A more general analysis is possible in principle and would be of interest but lies beyond our present scope.

In cartesian coordinates and for $d = 4$, the modification to the effective refractive index in the laboratory frame can be written as

$$\zeta^0 = -\frac{1}{2}\hat{l}^j \hat{l}^k \tilde{\kappa}_{e-}^{jk} + \frac{1}{2}\epsilon^{jkl} \hat{l}^j \tilde{\kappa}_{o+}^{kl} + \tilde{\kappa}_{\text{tr}}^{\text{lab}}, \quad (11)$$

where the ten cartesian coefficients for Lorentz violation associated with nonbirefringent operators at $d = 4$, which are linearly related to the spherical coefficients, are taken as the symmetric combination $\tilde{\kappa}_{e-}^{JK}$, the antisymmetric combination $\tilde{\kappa}_{o+}^{JK}$, and the trace component $\tilde{\kappa}_{\text{tr}}$ in the Sun-centered frame [25]. This gives

$$\begin{aligned}\Delta\bar{n} &= -\frac{1}{2}(\hat{l}_1^j \hat{l}_1^k - \hat{l}_2^j \hat{l}_2^k) \tilde{\kappa}_{e-}^{jk} \\ &= -\frac{1}{2}(\hat{l}_1^j \hat{l}_1^k - \hat{l}_2^j \hat{l}_2^k) (\Lambda^j{}_J \Lambda^k{}_K \tilde{\kappa}_{e-}^{JK} + \Lambda^j{}_T \Lambda^k{}_J \epsilon^{JKL} \tilde{\kappa}_{o+}^{KL} \\ &\quad - 2\Lambda^j{}_T \Lambda^k{}_K \tilde{\kappa}_{\text{tr}}).\end{aligned}\quad (12)$$

In this expression, the elements of the Lorentz transformation relating the Sun-centered frame and the laboratory frame can be taken as

$$\Lambda^0{}_T = 1, \quad \Lambda^0{}_J = -\beta^J, \quad \Lambda^j{}_T = -(R \cdot \vec{\beta})^j, \quad \Lambda^j{}_J = R^{jJ}, \quad (13)$$

where the matrix R^{jJ} rotating between the Sun-centered and laboratory frames is given by Eq. (C1) of Ref. [25], and β^J is given in terms of the orbital and laboratory boosts by Eq. (C2) of the same reference.

The above set of equations suffices to determine the explicit form of $\Delta\bar{n}$ in terms of $d = 4$ cartesian coefficients for Lorentz violation, once the location and relevant properties of the observatory are specified. The cartesian coefficients can then be transformed into spherical ones if desired. For example, for the Hanford site the explicit contributions for each harmonic in terms of spherical coefficients for Lorentz violation in the Sun-centered frame are displayed in Table 2. In this table, the first column specifies the harmonic. All relevant harmonics involving the sidereal and annual frequencies, including their sidebands, are considered. The second column gives the parity-even contributions, which match those shown in Table 1. The parity-odd contributions, which are proportional to one power of the boost, are presented in the third column. The final column provides the contributions involving the isotropic coefficient $c_{(I)00}^{(4)}$, all of which are parity even and involve two powers of the boost.

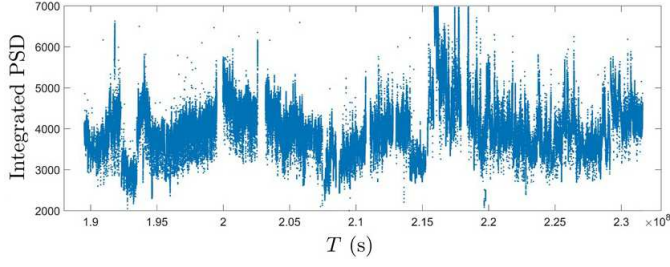


Figure 1: Integrated fsr PSD as a function of time T in the Sun-centered frame.

Note that all nine independent components $c_{(I)\mu\nu}^{(4)}$ appear. However, the component $c_{(I)20}^{(4)}$ contributes only to the constant term, which lacks a characteristic time variation and can therefore be expected to be more challenging to detect. Note also that the sole contribution to the twice-annual harmonic comes from the isotropic coefficient.

To investigate the experimental reach attainable in practice, we analyze the preliminary dataset taken in the fsr channel at the Hanford site during the S5 LIGO run, over the 16-month period from March 31, 2006 to July 31, 2007 [15]. During this run, the photodetector signal was demodulated at 37.52 kHz. The power spectral density (PSD), which is proportional to the absolute value of the electric-field amplitude squared per Hz, was evaluated over intervals of 64 s and then integrated in the range 37.52 ± 0.2 kHz, thereby yielding a time series of the power at the fsr frequency. Figure 1 shows this series. The vertical axis is the uncalibrated integrated PSD, while the horizontal axis is the time T in seconds since the vernal equinox 2000. The time series corresponds to the squared modulus $|\phi_b + \phi_s|^2$, where ϕ_b is the bias phase shift mentioned above and ϕ_s is the time-dependent phase shift induced by the time variations in $\Delta\bar{n}$. Note that these data provide an essentially continuous record over the 16-month period. This represents another advantage of the fsr channel in that it provides continuity over this extended period, whereas the carrier channel is reset after the interferometer loses lock, typically after about 24 hours.

To study the various sidereal and annual signals, the power spectra in the appropriate frequency ranges can be extracted from the dataset. The resolution bandwidth is approximately 2.4×10^{-8} Hz. The PSD as a function of frequency in the sidereal region is shown in Fig. 2. Table 3 lists the frequencies and the PSD values for each of the four prominent peaks. Four tidal lines are known to appear in this region: the lunar principle wave O_1 , the solar principle wave P_1 , the lunar and solar declinational waves K_1 , and the solar elliptical wave S_1 of K_1 . Near the twice-sidereal frequency, the power spectrum is presented in Fig. 3, and the locations and sizes of the four prominent peaks are provided in Table 3. Again, four tidal lines are known here: the lunar principle wave M_2 , the solar principle wave S_2 , the lunar major elliptical wave N_2 of M_2 , and the lunar and solar declinational waves K_2 . With one exception, the frequencies of the four prominent peaks in each of these spectra match the locations of these tidal lines to 10^{-8} Hz. The measured power in each line is proportional to the tidal amplitude because it arises

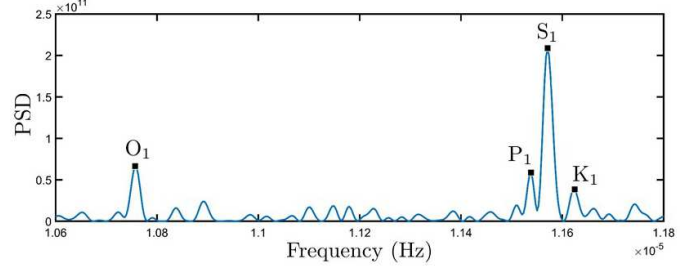


Figure 2: PSD versus frequency in the sidereal region.

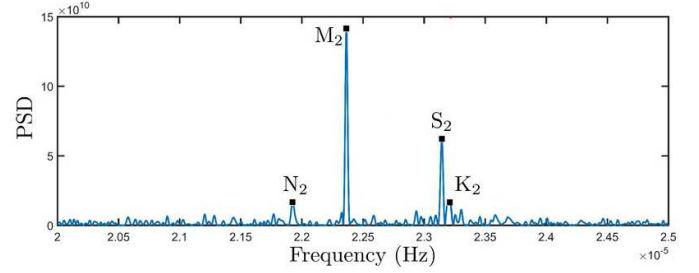


Figure 3: PSD versus frequency in the semisidereal region.

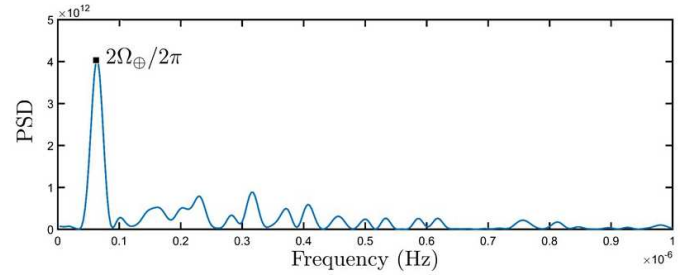


Figure 4: PSD versus frequency in the annual region.

from interference, and the observed relative amplitudes agree with known values [17]. The exception is the S_1 line, which is shifted by about 2.5 standard deviations from the expected frequency and should be unobservable. This line must therefore be attributed to human activities on a daily cycle.

The PSD in the vicinity of the solar frequency is displayed in Fig. 4. No significant annual modulation appears in the data. However, a pronounced peak is visible at the frequency $f = (6.5 \pm 0.6) \times 10^{-8}$ Hz, which is consistent with the semi-annual frequency $2\Omega_{\oplus}/2\pi \approx 6.2 \times 10^{-8}$ Hz. The amplitude of the declinational solar tidal wave at this frequency is too small by more than an order of magnitude to account for this peak, which has height as shown in Table 3. The origin of this anomalous peak is currently unknown but could be instrumental. As an illustration of principle, consider the feed-forward servo mechanism that helps to maintain the interferometer lock by correcting for the tidal deformation of the Earth via actuators that modify the macroscopic arm-length difference. This servo includes a correction at twice the annual frequency, which conceivably could be a natural source of an instrumental effect.

Harmonic	$d = 4$ contributions	$d = 6$ contributions ($\times 10^{-18}$ GeV ²)
1	$0.14 c_{(I)20}^{(4)}$	$0.19 c_{(I)20}^{(6)} - 0.28 c_{(I)40}^{(6)}$
$\cos(\omega_{\oplus} T_{\oplus})$	$0.24 \text{Re } c_{(I)21}^{(4)} - 1.0 \text{Im } c_{(I)21}^{(4)}$	$0.32 \text{Re } c_{(I)21}^{(6)} + 0.062 \text{Re } c_{(I)41}^{(6)} - 1.4 \text{Im } c_{(I)21}^{(6)} + 1.1 \text{Im } c_{(I)41}^{(6)}$
$\sin(\omega_{\oplus} T_{\oplus})$	$-1.0 \text{Re } c_{(I)21}^{(4)} - 0.24 \text{Im } c_{(I)21}^{(4)}$	$-1.4 \text{Re } c_{(I)21}^{(6)} + 1.1 \text{Re } c_{(I)41}^{(6)} - 0.32 \text{Im } c_{(I)21}^{(6)} - 0.062 \text{Im } c_{(I)41}^{(6)}$
$\cos(2\omega_{\oplus} T_{\oplus})$	$0.36 \text{Re } c_{(I)22}^{(4)} - 1.1 \text{Im } c_{(I)22}^{(4)}$	$0.49 \text{Re } c_{(I)22}^{(6)} + 0.061 \text{Re } c_{(I)42}^{(6)} - 1.4 \text{Im } c_{(I)22}^{(6)} - 0.82 \text{Im } c_{(I)42}^{(6)}$
$\sin(2\omega_{\oplus} T_{\oplus})$	$-1.1 \text{Re } c_{(I)22}^{(4)} - 0.36 \text{Im } c_{(I)22}^{(4)}$	$-1.4 \text{Re } c_{(I)22}^{(6)} - 0.82 \text{Re } c_{(I)42}^{(6)} - 0.49 \text{Im } c_{(I)22}^{(6)} - 0.061 \text{Im } c_{(I)42}^{(6)}$
$\cos(3\omega_{\oplus} T_{\oplus})$	—	$0.27 \text{Re } c_{(I)43}^{(6)} - 0.64 \text{Im } c_{(I)43}^{(6)}$
$\sin(3\omega_{\oplus} T_{\oplus})$	—	$-0.64 \text{Re } c_{(I)43}^{(6)} - 0.27 \text{Im } c_{(I)43}^{(6)}$
$\cos(4\omega_{\oplus} T_{\oplus})$	—	$-0.27 \text{Re } c_{(I)44}^{(6)} + 0.78 \text{Im } c_{(I)44}^{(6)}$
$\sin(4\omega_{\oplus} T_{\oplus})$	—	$0.78 \text{Re } c_{(I)44}^{(6)} + 0.27 \text{Im } c_{(I)44}^{(6)}$

Table 1: Contributions from sidereal harmonics for $d = 4$ and $d = 6$ at Hanford, WA.

Harmonic	Parity-even	Parity-odd ($\times 10^{-5}$)	Isotropic ($\times 10^{-10}$)
1	$0.14 c_{(I)20}^{(4)}$	$0.068 c_{(I)10}^{(4)}$	$-1.2 c_{(I)00}^{(4)}$
$\cos(\Omega_{\oplus} T)$	—	$0.56 c_{(I)10}^{(4)} - 0.92 \text{Im } c_{(I)11}^{(4)}$	$0.12 c_{(I)00}^{(4)}$
$\sin(\Omega_{\oplus} T)$	—	$-1.0 \text{Re } c_{(I)11}^{(4)}$	—
$\cos(2\Omega_{\oplus} T)$	—	—	$0.36 c_{(I)00}^{(4)}$
$\sin(2\Omega_{\oplus} T)$	—	—	—
$\cos(\omega_{\oplus} T_{\oplus} - 2\Omega_{\oplus} T)$	—	—	$-5.2 c_{(I)00}^{(4)}$
$\sin(\omega_{\oplus} T_{\oplus} - 2\Omega_{\oplus} T)$	—	—	$-1.2 c_{(I)00}^{(4)}$
$\cos(\omega_{\oplus} T_{\oplus} - \Omega_{\oplus} T)$	—	$-6.1 c_{(I)10}^{(4)} + 0.42 \text{Re } c_{(I)11}^{(4)} - 1.8 \text{Im } c_{(I)11}^{(4)}$	$0.13 c_{(I)00}^{(4)}$
$\sin(\omega_{\oplus} T_{\oplus} - \Omega_{\oplus} T)$	—	$-1.4 c_{(I)10}^{(4)} - 1.8 \text{Re } c_{(I)11}^{(4)} - 0.42 \text{Im } c_{(I)11}^{(4)}$	$-0.30 c_{(I)00}^{(4)}$
$\cos(\omega_{\oplus} T_{\oplus})$	$0.24 \text{Re } c_{(I)21}^{(4)} - 1.0 \text{Im } c_{(I)21}^{(4)}$	$0.10 \text{Re } c_{(I)11}^{(4)} + 0.046 \text{Im } c_{(I)11}^{(4)}$	$-5.0 c_{(I)00}^{(4)}$
$\sin(\omega_{\oplus} T_{\oplus})$	$-1.0 \text{Re } c_{(I)21}^{(4)} - 0.24 \text{Im } c_{(I)21}^{(4)}$	$0.046 \text{Re } c_{(I)11}^{(4)} - 0.10 \text{Im } c_{(I)11}^{(4)}$	$-1.2 c_{(I)00}^{(4)}$
$\cos(\omega_{\oplus} T_{\oplus} + \Omega_{\oplus} T)$	—	$0.26 c_{(I)10}^{(4)} + 0.42 \text{Re } c_{(I)11}^{(4)} - 1.8 \text{Im } c_{(I)11}^{(4)}$	$-0.0057 c_{(I)00}^{(4)}$
$\sin(\omega_{\oplus} T_{\oplus} + \Omega_{\oplus} T)$	—	$0.062 c_{(I)10}^{(4)} - 1.8 \text{Re } c_{(I)11}^{(4)} - 0.42 \text{Im } c_{(I)11}^{(4)}$	$0.013 c_{(I)00}^{(4)}$
$\cos(\omega_{\oplus} T_{\oplus} + 2\Omega_{\oplus} T)$	—	—	$0.22 c_{(I)00}^{(4)}$
$\sin(\omega_{\oplus} T_{\oplus} + 2\Omega_{\oplus} T)$	—	—	$0.053 c_{(I)00}^{(4)}$
$\cos(2\omega_{\oplus} T_{\oplus} - 2\Omega_{\oplus} T)$	—	—	$-4.5 c_{(I)00}^{(4)}$
$\sin(2\omega_{\oplus} T_{\oplus} - 2\Omega_{\oplus} T)$	—	—	$13 c_{(I)00}^{(4)}$
$\cos(2\omega_{\oplus} T_{\oplus} - \Omega_{\oplus} T)$	—	$-9.1 \text{Re } c_{(I)11}^{(4)} - 3.1 \text{Im } c_{(I)11}^{(4)}$	—
$\sin(2\omega_{\oplus} T_{\oplus} - \Omega_{\oplus} T)$	—	$-3.1 \text{Re } c_{(I)11}^{(4)} + 9.1 \text{Im } c_{(I)11}^{(4)}$	—
$\cos(2\omega_{\oplus} T_{\oplus})$	$0.36 \text{Re } c_{(I)22}^{(4)} - 1.1 \text{Im } c_{(I)22}^{(4)}$	—	$0.39 c_{(I)00}^{(4)}$
$\sin(2\omega_{\oplus} T_{\oplus})$	$-1.1 \text{Re } c_{(I)22}^{(4)} - 0.36 \text{Im } c_{(I)22}^{(4)}$	—	$-1.1 c_{(I)00}^{(4)}$
$\cos(2\omega_{\oplus} T_{\oplus} + \Omega_{\oplus} T)$	—	$0.39 \text{Re } c_{(I)11}^{(4)} + 0.13 \text{Im } c_{(I)11}^{(4)}$	—
$\sin(2\omega_{\oplus} T_{\oplus} + \Omega_{\oplus} T)$	—	$0.13 \text{Re } c_{(I)11}^{(4)} - 0.39 \text{Im } c_{(I)11}^{(4)}$	—
$\cos(2\omega_{\oplus} T_{\oplus} + 2\Omega_{\oplus} T)$	—	—	$-0.0083 c_{(I)00}^{(4)}$
$\sin(2\omega_{\oplus} T_{\oplus} + 2\Omega_{\oplus} T)$	—	—	$0.024 c_{(I)00}^{(4)}$

Table 2: Contributions from $d = 4$ spherical coefficients at Hanford, WA.

Peak	Frequency	Power spectral density
O_1	1.076×10^{-5}	6.655×10^{10}
P_1	1.154×10^{-5}	5.869×10^{10}
S_1	1.157×10^{-5}	2.088×10^{11}
K_1	1.162×10^{-5}	3.841×10^{10}
N_2	2.192×10^{-5}	1.666×10^{10}
M_2	2.236×10^{-5}	1.415×10^{11}
S_2	2.315×10^{-5}	6.218×10^{10}
K_2	2.321×10^{-5}	1.657×10^{10}
$2\Omega_{\oplus}/2\pi$	6.239×10^{-8}	4.034×10^{12}

Table 3: Frequencies (Hz) and power spectral density of selected peaks.

Harmonic	$\Delta\bar{n}/\bar{n}$
ω_{\oplus}	$< 1.4 \times 10^{-20}$
$2\omega_{\oplus}$	$< 2.0 \times 10^{-22}$
$3\omega_{\oplus}$	$< 2.1 \times 10^{-22}$
$4\omega_{\oplus}$	$< 2.1 \times 10^{-22}$
Ω_{\oplus}	$< 3.4 \times 10^{-20}$
$2\Omega_{\oplus}$	$(4.0 \pm 0.25) \times 10^{-19}$

Table 4: Results for $\Delta\bar{n}/\bar{n}$ from Hanford, WA preliminary data.

However, in practice the tidal servo would have been reset between the lock periods roughly once a day, and moreover the size of the correction is too small by more than an order of magnitude, so this appears unlikely to be the source of the observed continuous modulation. In the analysis that follows, we include the anomalous peak for completeness, but its definitive interpretation and verification must await the acquisition of an independent dataset.

To calibrate the power spectra, we take advantage of the strongest tidal line in the twice-sidereal region, which is the lunar principle wave M_2 . The horizontal gravity gradients from this wave are known [27]. They can be used to calculate the induced phase shift on the light at the detector port, given the latitude of the Hanford detector and the orientation of the interferometer arms. This derived value is in close agreement with the result obtained from the observed modulation of the data and a simulation of the inteferometer [17, 28]. Normalizing the spectrum to this phase shift yields $\Delta\phi/2\pi = (1.1 \pm 1.2) \times 10^{-12}$ for a single traversal at this frequency. We can use this to extract the values of $\Delta\bar{n}/\bar{n}$ at the various harmonics of ω_{\oplus} and Ω_{\oplus} of interest.

The results of this procedure are shown in Table 4. The value for each of ω_{\oplus} , $2\omega_{\oplus}$, and Ω_{\oplus} is a 2σ confidence limit on a signal above expectation, while that for each of $3\omega_{\oplus}$ and $4\omega_{\oplus}$ is a 2σ confidence limit on a signal above noise. The 16σ signal at $2\Omega_{\oplus}$ is obtained from the anomalous peak discussed above. In principle, the phases of the oscillations and also the various sidebands presented in Table 2 contain interesting information

Harmonic	Coefficient	Result
ω_{\oplus}	$ c_{(J)21}^{(4)} $	$< 1.3 \times 10^{-20}$
	$ c_{(J)21}^{(6)} $	$< 1.0 \times 10^{-2} \text{ GeV}^{-2}$
	$ c_{(J)41}^{(6)} $	$< 1.3 \times 10^{-2} \text{ GeV}^{-2}$
$2\omega_{\oplus}$	$ c_{(J)22}^{(4)} $	$< 1.8 \times 10^{-22}$
	$ c_{(J)22}^{(6)} $	$< 1.3 \times 10^{-4} \text{ GeV}^{-2}$
	$ c_{(J)42}^{(6)} $	$< 2.4 \times 10^{-4} \text{ GeV}^{-2}$
$3\omega_{\oplus}$	$ c_{(J)43}^{(6)} $	$< 3.0 \times 10^{-4} \text{ GeV}^{-2}$
$4\omega_{\oplus}$	$ c_{(J)44}^{(6)} $	$< 2.6 \times 10^{-4} \text{ GeV}^{-2}$
Ω_{\oplus}	$ c_{(J)00}^{(4)} $	$< 3.3 \times 10^{-9}$
	$ c_{(J)10}^{(4)} $	$< 6.7 \times 10^{-15}$
	$ \text{Re } c_{(J)11}^{(4)} $	$< 3.8 \times 10^{-15}$
	$ \text{Im } c_{(J)11}^{(4)} $	$< 4.1 \times 10^{-15}$

Table 5: Results for spherical coefficients from Hanford, WA preliminary data.

about Lorentz violation as well. However, for the given duration of the run, the resolution is insufficient to extract useful information about these sidebands.

Combining the values in Table 4 with the contributions to $\Delta\bar{n}/\bar{n}$ presented in Tables 1 and 2 yields results for the spherical coefficients for Lorentz violation. To gain some insight into these results, we can follow standard procedure in the field [4] and consider the result for each spherical coefficient in turn under the assumption that all others vanish. These results are collected in Table 5. Additional insight is obtained by working instead in a cartesian basis. Results for the $d = 4$ cartesian coefficients $\tilde{\kappa}_{e-}^{JK}$, $\tilde{\kappa}_{o+}^{JK}$, and $\tilde{\kappa}_{tr}$ are displayed in Table 6.

Overall, the results in Tables 5 and 6 reveal improvements in laboratory sensitivity to all but one of the coefficients for Lorentz violation associated with operators at $d = 4$. The limits on coefficients controlling parity-even rotation-violating operators represent a gain of about four orders of magnitude over existing laboratory bounds [4, 12–14], while those on parity-odd operators are improved by about a factor of four. In contrast, the constraint on $\tilde{\kappa}_{tr}$ in Table 6 is weaker than the best existing two-sided bounds from laboratory experiments [4, 29, 30] and from astrophysics [4, 31]. Moreover, a definitive measurement of the $d = 4$ coefficient $c_{(J)00}^{(4)}$ or, equivalently, $\tilde{\kappa}_{tr}$ cannot be inferred from these results as the constraint obtained from the annual frequency Ω_{\oplus} appears incompatible with the observed signal from the anomalous peak at $2\Omega_{\oplus}$. Assuming an appropriate phase at this frequency yields the results $|c_{(J)00}^{(4)}| = (11.1 \pm 0.7) \times 10^{-9}$ and $|\tilde{\kappa}_{tr}| = (3.1 \pm 0.2) \times 10^{-9}$. This anomalous signal could conceivably be a theoretical artifact of the analysis performed here, which assumes conventional fermions and therefore is insensitive to matter-sector coefficients producing distinct effects at the annual and semianual frequencies [32], but the possibility of an instrumental systematic means that a compelling resolution of this discrepancy is unlikely to be attained in the absence of new data. The results

Harmonic	Coefficient	Result
ω_{\oplus}	$ \tilde{\kappa}_{e-}^{XZ} $	$< 2.1 \times 10^{-20}$
	$ \tilde{\kappa}_{e-}^{YZ} $	$< 2.1 \times 10^{-20}$
$2\omega_{\oplus}$	$ \tilde{\kappa}_{e-}^{XY} $	$< 2.7 \times 10^{-22}$
	$ \tilde{\kappa}_{e-}^{XX} - \tilde{\kappa}_{e-}^{YY} $	$< 5.5 \times 10^{-22}$
Ω_{\oplus}	$ \tilde{\kappa}_{tr} $	$< 9.2 \times 10^{-10}$
	$ \tilde{\kappa}_{o+}^{XY} $	$< 6.6 \times 10^{-15}$
	$ \tilde{\kappa}_{o+}^{XZ} $	$< 5.7 \times 10^{-15}$
	$ \tilde{\kappa}_{o+}^{YZ} $	$< 5.2 \times 10^{-15}$

Table 6: Results for minimal cartesian coefficients from Hanford, WA.

in Table 5 also represent the first laboratory bounds obtained on the coefficients $c_{(I)jm}^{(6)}$, albeit at a reduced sensitivity compared to limits found in studies of the dispersion of light from astrophysical sources [33].

The striking improvement in sensitivity to photon-sector Lorentz violation revealed in the above analysis suggests that further searches using existing gravitational-wave detectors would be well worthwhile. Substantial further gains in sensitivity are likely to be attainable by implementing several options. One is to incorporate results from sites other than Hanford, including those for LIGO, Virgo, planned ground-based observatories, and perhaps eventually space-based missions such as LISA. A combined analysis would not only increase statistics and potentially eliminate systematics but would also gain from the differing colatitudes and orientations of the instruments. For example, a calculation of the contributions from various harmonics at the Livingston site reveals that the semiannual signal is enhanced by a factor of 4.2 due to the geometry of the site, which should permit confirmation or refutation of the anomalous peak. Another potential plus is the improved noise control now in place for the advanced LIGO instrument, which could imply a gain in sensitivity to Lorentz violation as well.

To summarize, we have shown in this work that the interferometers in gravitational-wave observatories can be used to perform exquisitely sensitive tests of Lorentz invariance in the photon sector, thereby extending the role of these instruments beyond the more direct searches for Lorentz violation in the propagation of gravitational waves [34] and other prospective studies of quantum gravity [35]. Searches of this type have a reach for photon-sector Lorentz violation that is several orders of magnitude beyond existing laboratory tests [4, 12–14], and substantial improvements in the results reported here can be envisaged. The future is evidently bright for improved studies of Lorentz invariance in the spirit of the pioneering Michelson-Morley experiment.

Acknowledgments

The preliminary data discussed here were obtained during the LIGO S5 run. We are indebted to the staff and operators of the Hanford LIGO Observatory and to the members of the

LIGO Scientific Collaboration for their dedicated efforts before and during the run. In particular, we thank W.E. Butler, C. Forrest, T. Fricke, S. Giampanis, F.J. Raab, and D. Sigg, who designed, installed, and operated the fsr channel and analyzed the data. LIGO is operated by Caltech and MIT and is funded by the United States National Science Foundation. The authors were supported in part by the United States Department of Energy under grants DE-SC0010120 and DE-FG02-91ER40685, by the United States National Science Foundation under grants PHY-1520570 and PHY-0456239, and by the Indiana University Center for Spacetime Symmetries.

References

- [1] A.A. Michelson and E.W. Morley, *Am. J. Sci.* **34**, 333 (1887); *Phil. Mag.* **24**, 449 (1887).
- [2] R.J. Kennedy and E.M. Thorndike, *Phys. Rev.* **42**, 400 (1932).
- [3] V.A. Kostelecký and S. Samuel, *Phys. Rev. D* **39**, 683 (1989); V.A. Kostelecký and R. Potting, *Nucl. Phys. B* **359**, 545 (1991); *Phys. Rev. D* **51**, 3923 (1995).
- [4] V.A. Kostelecký and N. Russell, *Data Tables for Lorentz and CPT Violation*, 2016 edition, arXiv:0801.0287v9.
- [5] LIGO Scientific Collaboration and Virgo Collaboration, B.P. Abbott *et al.*, *Phys. Rev. Lett.* **116**, 061102 (2016).
- [6] B.P. Abbott *et al.*, *Rep. Prog. Phys.* **72**, 076901 (2009).
- [7] F. Acernese *et al.*, *J. Opt. A* **10**, 064009 (2008).
- [8] B. Willke *et al.*, *Class. Quantum Grav.* **19**, 1377 (2002).
- [9] K. Somiya, *Class. Quantum Grav.* **29**, 124007 (2012).
- [10] C.S. Unnikrishnan, *Int. J. Mod. Phys. D* **22**, 1341010 (2013).
- [11] M. Armano *et al.*, *J. Phys. Conf. Ser.* **610**, 012005 (2015).
- [12] Q. Chen, E. Magoulakis, and S. Schiller, *Phys. Rev. D* **93**, 022003 (2016).
- [13] M. Nagel *et al.*, *Nature Commun.* **6**, 8174 (2015).
- [14] T. Pruttivarasin *et al.*, *Nature* **517**, 592 (2015).
- [15] A.C. Melissinos, for the LIGO Scientific Collaboration, in T. Damour, R.T. Jantzen, and R. Ruffini, eds., *Proceedings of the 12th Marcel Grossmann Meeting on General Relativity*, World Scientific, Singapore, 2011, p. 1718 [arXiv:1001.0558].
- [16] A.V. Gusev, V.N. Rudenko, and I.S. Yudin, *JETP* **119**, 687 (2014) [arXiv:1310.3104].
- [17] A.C. Melissinos, arXiv:1410.0854.
- [18] See, for example, S. Weinberg, *Proc. Sci.* **CD 09**, 001 (2009).
- [19] D. Colladay and V.A. Kostelecký, *Phys. Rev. D* **55**, 6760 (1997); *Phys. Rev. D* **58**, 116002 (1998).
- [20] V.A. Kostelecký, *Phys. Rev. D* **69**, 105009 (2004).
- [21] R. Bluhm, *Lect. Notes Phys.* **702**, 191 (2006).
- [22] J.D. Tasson, *Rep. Prog. Phys.* **77**, 062901 (2014).
- [23] Y. Bonder, *Phys. Rev. D* **91**, 125002 (2015); V.A. Kostelecký and J.D. Tasson, *Phys. Rev. D* **83**, 016013 (2011); V.A. Kostelecký and N. Russell, *Phys. Lett. B* **693**, 443 (2010); B. Altschul, *J. Phys. A* **39**, 13757 (2006); R. Lehnert, *Phys. Rev. D* **74**, 125001 (2006); Q.G. Bailey and V.A. Kostelecký, *Phys. Rev. D* **70**, 076006 (2004); D. Colladay and P. McDonald, *J. Math. Phys.* **43**, 3554 (2002); V.A. Kostelecký and R. Lehnert, *Phys. Rev. D* **63**, 065008 (2001).
- [24] V.A. Kostelecký and M. Mewes, *Ap. J.* **689**, L1 (2008); *Phys. Rev. D* **80**, 015020 (2009).
- [25] V.A. Kostelecký and M. Mewes, *Phys. Rev. D* **66**, 056005 (2002).
- [26] R. Bluhm, V.A. Kostelecký, C.D. Lane, and N. Russell, *Phys. Rev. D* **68**, 125008 (2003); *Phys. Rev. Lett.* **88**, 090801 (2002).
- [27] P. Melchior, *The Tides of the Planet Earth*, Pergamon Press, Oxford, 1978.
- [28] A. Freise, D. Brown, and C. Bond, arXiv:1306.2973.
- [29] B. Altschul, *Phys. Rev. D* **80**, 091901(R) (2009).
- [30] M.A. Hohensee, R. Lehnert, D.F. Phillips, and R.L. Walsworth, *Phys. Rev. D* **80**, 036010 (2009); *Phys. Rev. Lett.* **102**, 170402 (2009).
- [31] M. Schreck, in V.A. Kostelecký, ed., *CPT and Lorentz Symmetry IV*, World Scientific, Singapore 2008 [arXiv:1310.5159].
- [32] V.A. Kostelecký and M. Mewes, *Phys. Rev. D* **88**, 096006 (2013).
- [33] F. Kislak and H. Krawczynski, *Phys. Rev. D* **92**, 045016 (2015).

- [34] V.A. Kostelecký and J.D. Tasson, Phys. Lett. B **749**, 551 (2015); V.A. Kostelecký and M. Mewes, Phys. Lett. B **757**, 510 (2016); R. Tso and M. Zanolin, Phys. Rev. D **93**, 124033 (2016); M. Schreck, arXiv:1603.07452; N. Yunes, K. Yagi, and F. Pretorius, arXiv:1603.08955.
- [35] G. Amelino-Camelia, Phys. Rev. D **62**, 024015 (2000); Y.J. Ng and H. van Dam, Found. Phys. **30**, 795 (2000); G. Amelino-Camelia and C. Lämmerzahl, Class. Quantum Grav. **21**, 899 (2004); G. Sardin, arXiv:physics/0404116; X. Li and Z. Chang, Commun. Math. Phys. **60**, 535 (2013); O. Kwon and C.J. Hogan, Class. Quantum Grav. **33**, 105004 (2016).